

Diffraction Grating Scanners Using Polysilicon Micromotors

A. Azzam Yasseen, Steven W. Smith, Francis L. Merat, *Member, IEEE*, and Mehran Mehregany, *Member, IEEE*

Abstract—This paper describes polysilicon micromotors with single and pyramidal diffraction grating elements fabricated on the polished surface of large-area rotors for optical scanning applications. While taking full advantage of planar processing, such scanners have high-quality scan profiles, good efficiency, meter working distances, and multiple out of plane beam diffraction orders. Chemical-mechanical polishing was used to reduce the 5- μm -thick polysilicon rotors' average surface roughness from 420 Å to below 17 Å, with less than 1500-Å film removal, improving the optical performance of the gratings as well as the definition, delineation, and side wall quality of the device features. Self-assembled monolayers (SAM) were found to improve the overall micromotor's dynamic performance. SAM-coated scanners could operate at voltages as low as 15 V and maximum operational speeds of 5200 rpm. The gratings were tested optically at 633-nm wavelength and were verified to have spatial periods of 1.80 and 3.86 μm , closely matching their design values. Stepping and continuous mode dynamic operation of the scanners was demonstrated with visible diffraction orders at meter distances away.

Index Terms—Chemical-mechanical polishing, microactuators, micromotors, MOEMS, scanners.

I. INTRODUCTION

THERE is an increasing need in today's marketplace to develop low-cost high-precision optical scanners for a variety of applications. Scanners sample the two-dimensional space information in a predetermined manner to convert the original information into a stream of elements of various optical intensities to make it available for electronic manipulation [1]. As a result of recent progress in polysilicon micromotor development, the technology has advanced toward optical applications [2]. A 20- μm -tall reflective nickel polygon, plated on the surface of a polysilicon micromotor for in-plane scanning, was demonstrated in [2]. Scanners using micromotors whose rotors are 200- μm -thick reflective polygons were also reported [3].

A micromechanical scanner implementation has the potential to reduce the weight and size of existing scanners by orders of magnitude with significant decrease in cost due to batch fabrication [4]. Potential applications include bar code scanners, high speed optical switches, multiplexers, and

Manuscript received June 19, 1998; revised September 8, 1998. This work was supported in part by the Defense Advanced Research Projects Agency under Contract F49620-94-0007 and by the National Science Foundation under Grant ECS-9109343.

The authors are with the Microfabrication Laboratory, Department of Electrical Engineering and Computer Science, Case Western Reserve University, Cleveland, OH 44106 USA.

Publisher Item Identifier S 1077-260X(99)01273-3.

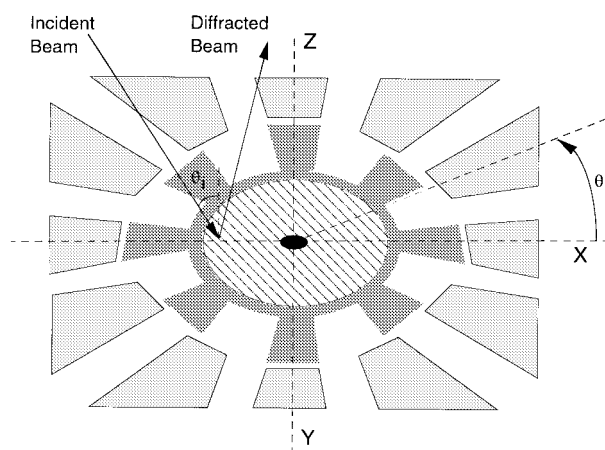


Fig. 1. Schematic of the operation of a salient-pole microscanner. (The rotor is in the x - y plane, while the z -axis is normal to the rotor.)

computer interconnects, among others. This paper presents a planar diffraction grating scanner incorporating reflective gratings on the rotor of wobble and salient-pole polysilicon micromotors [5]. Illuminating a reflective diffraction grating element with an incident laser results in multiple out-of-plane diffraction orders. With these diffraction gratings on the surface of a micromotor, out-of-plane scanning can be realized without the need for microoptics.

II. MICROSCANNER DESIGN

The planar diffraction grating scanners incorporate a reflective grating element on the rotor of a polysilicon micromotor permitting out-of-plane scanning. Fig. 1 presents a schematic drawing of a diffraction grating microscanner with an optically reflective grating element on the rotor. The fabrication process can be implemented by polysilicon surface micromachining, benefiting from low cost due to batch-fabrication, high rotating speeds, and small size. The IC compatibility of surface micromachining permits integration with on-chip drive and control electronics.

Optical Design

The design requires the fabrication of micromotors with large-area disk rotors to minimize optical diffraction. The large-area disk rotors should be solid with no release holes to minimize undesirable diffraction patterns. Chemical-mechanical polishing (CMP) of the polysilicon rotor surface is required for improved feature definition and delineation (e.g.,

TABLE I
SCANNER MICROMOTOR DIMENSIONS

Scanner Micromotor Parameter	Value
Rotor/Stator thickness (μm)	5.5
Rotor Diameter (mm)	0.5
Rotor/Stator Gap (μm)	1 and 2
Bearing Diameter (μm)	50
Bearing Clearance (μm)	0.5

fabrication of gratings with lines and spaces as small as $1 \mu\text{m}$, and good optical characteristics (e.g., surface reflectivity).

Such microscanners can be fabricated with planar single and pyramidal grating elements (i.e., an element consisting of four pie-shaped regions with adjacent regions having orthogonal line orientation) etched into the surface of the rotor with the grating spatial periods designed to be 2 and $4 \mu\text{m}$. The etch depth was chosen to maximize the intensity into a desired diffraction order for the incident light wavelength [6]. The diffraction grating profile may be designed to produce multiple diffracted beams for scanning at different focal lengths and angles. Illuminated single element gratings produce a row of diffraction orders spaced at angles given by [7]

$$\theta_q = \theta_i + q \frac{\lambda}{\Lambda}, \quad q = 0, \pm 1, \pm 2, \dots$$

where θ_i denotes the angle of the incident beam relative to the grating normal, q is the diffraction order, λ is the wavelength of the incident light, and Λ is the grating period. Only reflection mode gratings were considered in this paper. A multifaceted pyramidal grating as described above can yield two perpendicular rows of diffraction orders that can be used for scanning. As the motor rotates, the diffracted scanned-beam k vector's components change by [1]

$$\begin{aligned} k_{dx} &= K \cdot \sin(\theta_r) \\ k_{dy} &= K \cdot \cos(\theta_r) - \sin(\theta_i) \\ k_{dz} &= \sqrt{1 - k_{dx}^2 - k_{dy}^2} \end{aligned}$$

where k_{dx} , k_{dy} , and k_{dz} are the components of the diffracted beam's k vector along the x , y , and z axes, respectively, θ_r is the rotation angle of the diffraction grating in the x - y plane (as shown in Fig. 1), and K is the ratio of the optical wavelength and the grating period, λ/Λ .

Mechanical Design

The mechanical design of the microscanner is an extension of the micromotors resulting from the three-mask process described in [8]. Optical characteristics requirements and fabrication issues impose additional constraints on the micromotor design. As mentioned above, the optical design requires relatively large rotors with no release holes. As a result, these motors require extended release times during which the bearing and stator poles would be released if not anchored to the substrate. The rotor/stator polysilicon films are required to be relatively thick to provide the sufficient mechanical stiffness to prevent out-of-plane warping of the large-area rotors due to residual stress in polysilicon. Table I presents the important scanner micromotor dimensions.

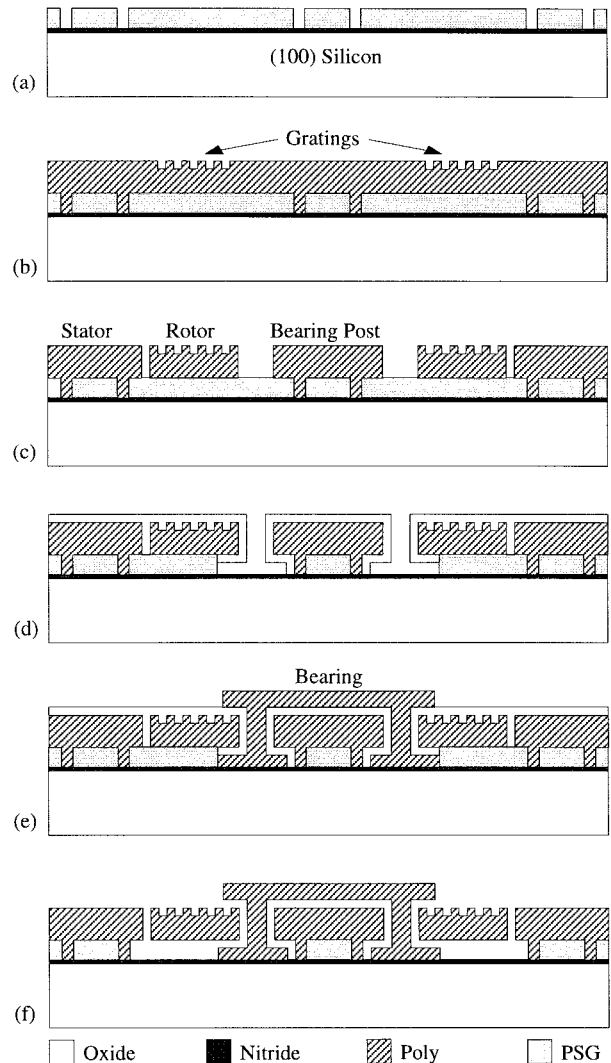
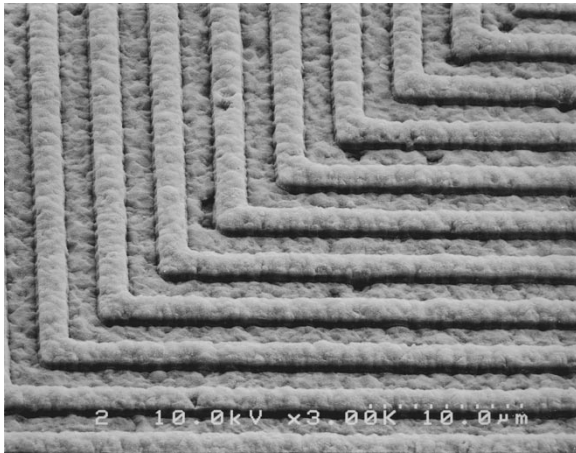


Fig. 2. Cross-sectional schematics describing the microscanner fabrication process. (a) After anchor definition and patterning. (b) After grating definition and patterning. (c) After rotor/stator definition and patterning. (d) After bearing clearance oxidation. (e) After bearing definition and patterning. (f) Released device.

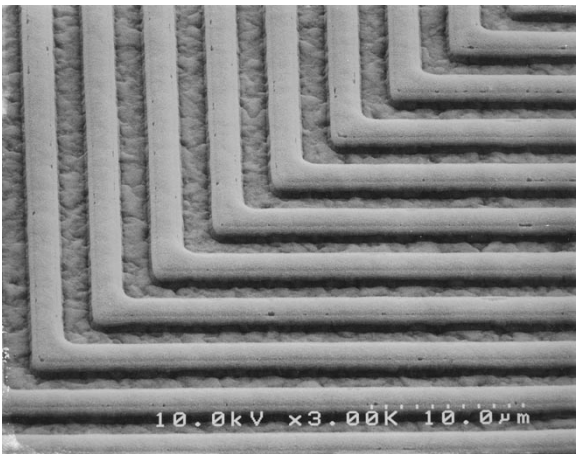
III. MICROSCANNER FABRICATION

A schematic description of the microscanner fabrication process is outlined in Fig. 2. Initially, 4500 \AA of LPCVD silicon nitride for electrical insulation, followed by $3.5 \mu\text{m}$ of PSG for a sacrificial layer, were deposited. The stator and the bearing post anchors were then patterned, followed by a $5.5\text{-}\mu\text{m}$ -thick rotor/stator LPCVD polysilicon deposition.

With increasing LPCVD polysilicon thickness, the film roughness increases due to increased grain size. Longer diffusion times were also needed to subsequently dope the polysilicon by thermal diffusion, further increasing the surface roughness. This inherent polysilicon surface roughness resulted in two limitations: 1) feature size definition and quality degradation and 2) undesirable optical scattering. High-quality optical surfaces must have a roughness value which is only a fraction of the wavelength of the light being transmitted, reflected, or refracted if large losses due to unnecessary scattering are to be avoided. A mirror surface finish is ob-



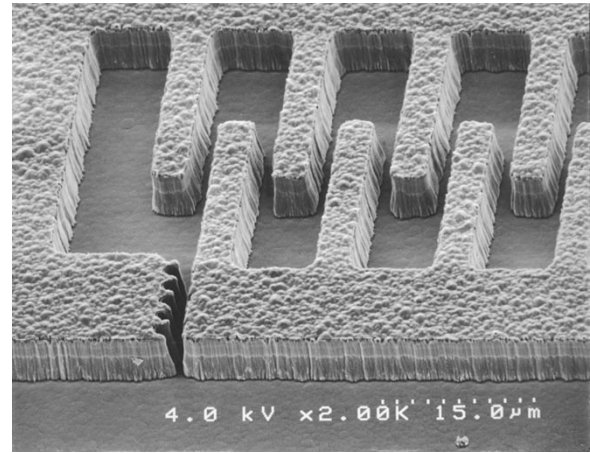
(a)



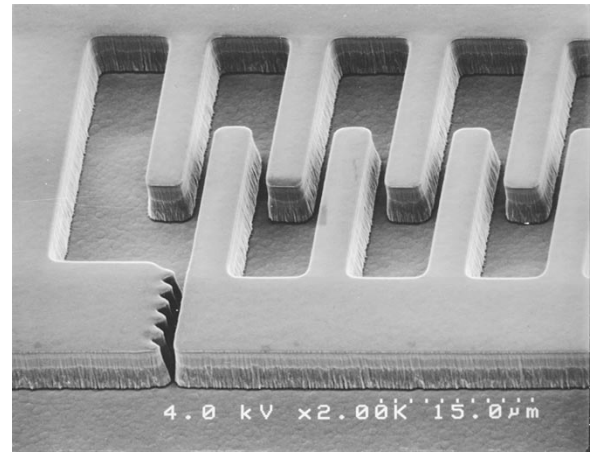
(b)

Fig. 3. SEM photos of $2\ \mu\text{m}$ lines and spaces diffraction gratings fabricated on (a) unpolished polysilicon and (b) polished polysilicon.

tained on polysilicon surfaces when R_a is reduced to below $40\ \text{\AA}$. Therefore, to produce high-quality optical surfaces, the average surface roughness (R_a) should be reduced to at least below $40\ \text{\AA}$. Fabrication of diffraction gratings also requires stringent line width control during photolithography and pattern delineation to obtain satisfactory optical performance. To meet these requirements, CMP was used to polish the surface of the polysilicon rotors on which the gratings were fabricated. With CMP, the average polysilicon surface roughness of the $5.5\text{-}\mu\text{m}$ -thick polysilicon films on which the gratings are fabricated was reduced from $420\ \text{\AA}$ to below $17\ \text{\AA}$ with less than $1500\text{-}\text{\AA}$ film removal [9]. Subsequent to CMP of the rotor/stator polysilicon, the gratings were patterned and etched into the polysilicon layer using an isotropic dry etch in order to approximate a sinusoidal grating profile for high optical diffraction efficiency [7]. Fig. 3 shows SEM profiles of gratings fabricated on unpolished and polished polysilicon motors. The two motors were otherwise processed identically. Notice the improvement in feature definition, as well as the smoothness of the polysilicon surfaces. Enhanced smoothness can be seen both at the top, as well as the bottom, of the gratings. Starting with rough polysilicon surfaces results in rough grating bottoms, while starting with smooth surfaces



(a)



(b)

Fig. 4. SEM photos of comb-finger structures fabricated from (a) unpolished polysilicon and (b) polished polysilicon.

results in smooth grating bottoms. In order to demonstrate CMP's effect on feature definition and delineation, a set of comb finger structures were fabricated from $5\text{-}\mu\text{m}$ -thick polysilicon layers. The resulting features from the polished and unpolished films are shown in Fig. 4. Substantial improvement in feature definition, line width resolution, side wall quality, and surface roughness is seen with the use of CMP.

Next, the rotor/stator pattern was defined and delineated using an anisotropic dry etch to produce rotor/stator gaps as small as $1\ \mu\text{m}$. The flange mold was then defined and etched, followed by a $0.5\text{-}\mu\text{m}$ bearing clearance oxidation. A $1\text{-}\mu\text{m}$ -thick polysilicon layer was deposited by LPCVD, heavily doped with phosphorus, and patterned to produce the bearing. SEM photos of typical diffraction grating wobble and salient-pole microscanners, are shown in Figs. 5 and 6, respectively.

IV. MICROSCANNER OPERATION

Mechanical Performance

Self-assembled monolayers (SAM) were reported to improve the performance of polysilicon micromotors [10]. When coating the scanner micromotors with OTS (C_{18}) SAM,

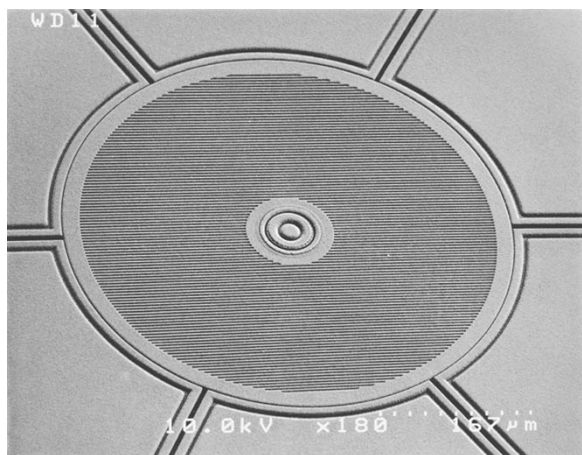


Fig. 5. Typical 500- μm -diameter wobble microscanner with polished rotor/stator polysilicon and single grating element of 3.86- μm period.

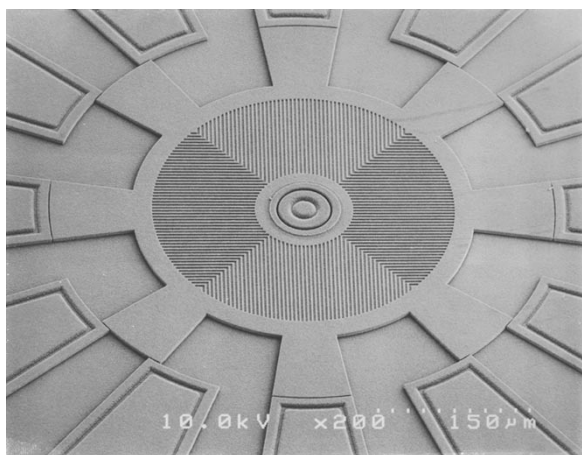


Fig. 6. Typical 500- μm -diameter salient-pole microscanner with polished rotor/stator polysilicon and pyramidal grating element of 3.86- μm period.

the microstructures emerged released and dry from the final rinse without requiring additional drying techniques. Spontaneous operation of the motors upon electrical excitation was achieved. The motors operated smoothly and reproducibly in room air for extended periods. The motors showed stable and repeatable operation over a testing period of more than one year. It was observed that high moisture levels in room air had an adverse effect on the operation of the OTS-coated scanner micromotors. Humidity above 45% was noticed to result in erratic motor operation.

Minimum operating voltages were as low as 15 and 45 V for wobble and salient-pole scanner micromotor designs, respectively. The maximum rotor speed of wobble micromotors was 7 rpm while the salient-pole micromotors achieved 5200 rpm. The 5200-rpm operating speed of the salient-pole scanner micromotor corresponds to 173 and 347 scans per second using the single and pyramidal diffraction elements, respectively. Fig. 7 shows typical step transient data for 500- μm -diameter 2- μm rotor/stator gap salient-pole scanner micromotors with and without OTS coating. The rise time of the step response for the OTS-coated motor is shorter than that without coating indicating that the coated motor experiences less friction in the

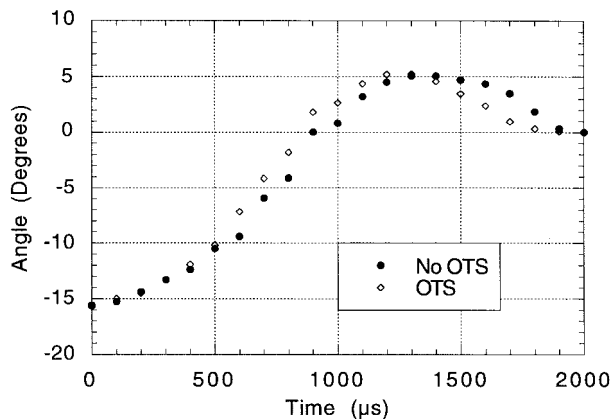


Fig. 7. Step transient data for 500- μm -diameter 2- μm -gap salient-pole scanner micromotor with and without OTS coating.

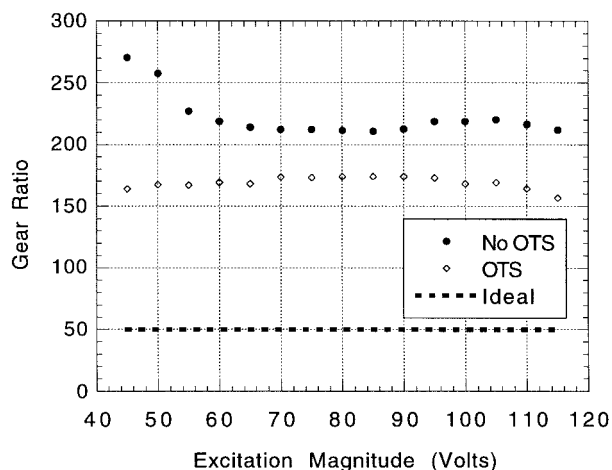


Fig. 8. Gear ratio as a function of excitation voltage for 500- μm -diameter 2- μm -gap wobble scanner micromotor with and without OTS coating.

flange. Fig. 8 shows the gear ratio as a function of excitation voltage for 500- μm -diameter 2- μm rotor/stator gap wobble scanner micromotor with and without OTS coating. The gear ratio for the coated scanner micromotors is close to the ideal gear ratio and is smaller than that without coating. This implies that OTS reduces, but not completely eliminates, slip in wobble scanner micromotors by increasing the friction in the bearing and reducing it at the flange as suggested by [10].

Static Optical Performance

Fig. 9 shows the test setup used for optical measurements. Fig. 10 shows the diffraction patterns obtained by illuminating single and pyramidal diffraction elements by an incident laser beam. The laser used throughout the optical measurements was a 20-mW unpolarized He-Ne of 633-nm wavelength. The optical properties of reflective diffraction gratings fabricated on polished and unpolished polysilicon rotors demonstrate the importance of polishing the rough polysilicon surfaces for optical applications. Fig. 11 demonstrates that CMP reduced the undesirable light scattering due to the excessive polysilicon surface roughness to values comparable to that achieved for gratings on single crystal silicon wafers. (For comparison, gratings were etched into single crystal silicon wafers, in

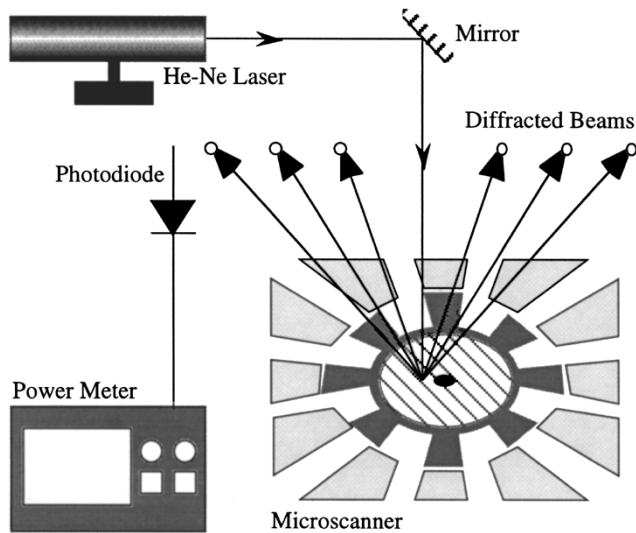
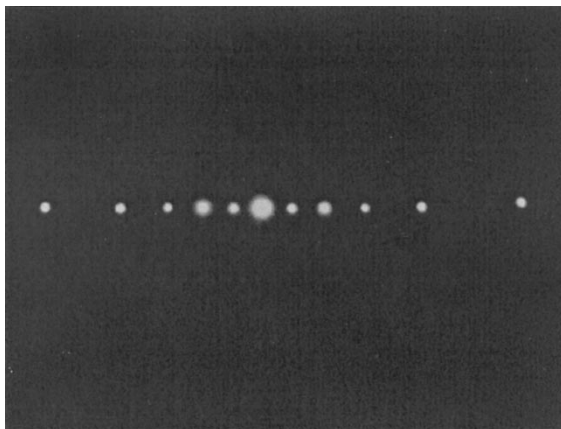
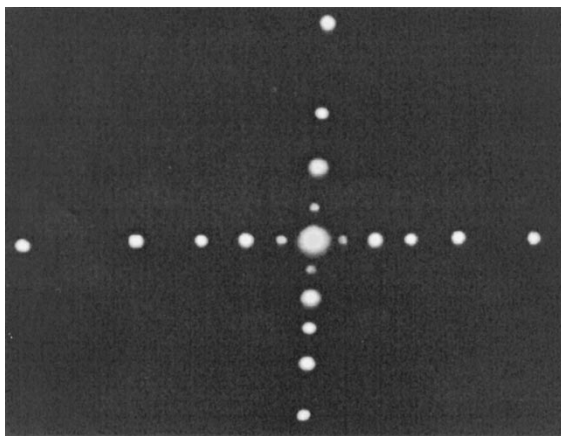


Fig. 9. Optical test setup for the diffraction grating microscanner testing.



(a)



(b)

Fig. 10. Diffraction pattern from grating elements fabricated in the polished rotor of the scanner micromotors. (a) Single. (b) Pyramidal.

addition to polished and unpolished polysilicon surfaces). The grating periods for the nominally 2- and 4- μm gratings were measured to be 1.80 and 3.86 μm , respectively. This result is in close correspondence with the target design, and the difference was attributed to variations in timed etching and

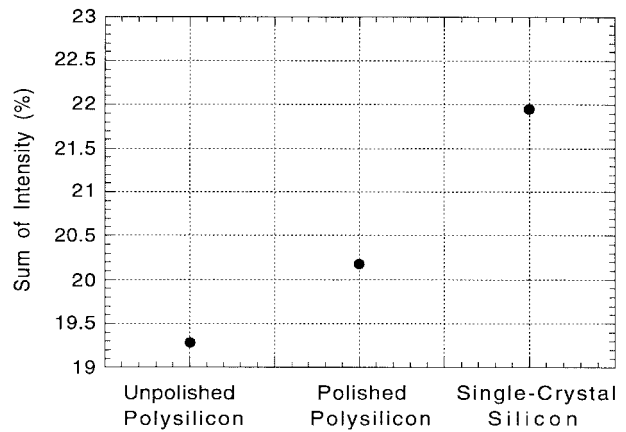


Fig. 11. Sum of intensity from all diffraction orders as percent of incident light from gratings fabricated on polished and unpolished polysilicon, as well as single-crystal silicon wafers.

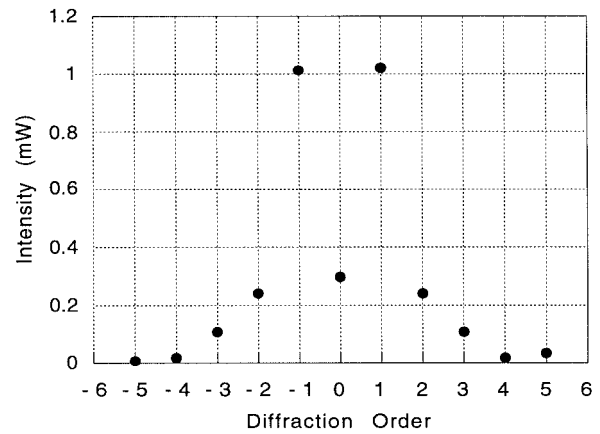


Fig. 12. Diffraction orders for a 3.86- μm period grating showing transfer of optical power from the zeroth- to the first-order spot.

photolithography. The grating etch depth can be adjusted to maximize intensity in a desired diffraction order (e.g., the first order) for a given incident optical wavelength. Fig. 12 demonstrates that adjusting the grating etch depth can be used to shift power from the zeroth order to higher diffraction orders.

Characterization of the diffracted laser beam profiles with a CCD camera indicated that at distances on the order of one meter from the microscanner, all diffraction orders provided Gaussian beam profiles, with gratings on polished polysilicon producing a higher degree of spatial uniformity and lower beam divergence than those on unpolished polysilicon. Fig. 13 compares measured beam intensity profiles and spot quality from similar gratings fabricated on unpolished and polished polysilicon rotors at 0.5-m distance from a grating microscanner using 633-nm laser. Note the increased intensity and reduced beam divergence as a result of polishing. The measured diffraction orders for 1.80- μm gratings were separated by $20.79^\circ \pm 0.62^\circ$ and those for the 3.86- μm gratings by $9.8^\circ \pm 0.53^\circ$. The line width and diffraction angles were uniform for similar gratings on the same wafer and between different wafers. Optical scanning at distances up to several meters without external optics was readily possible

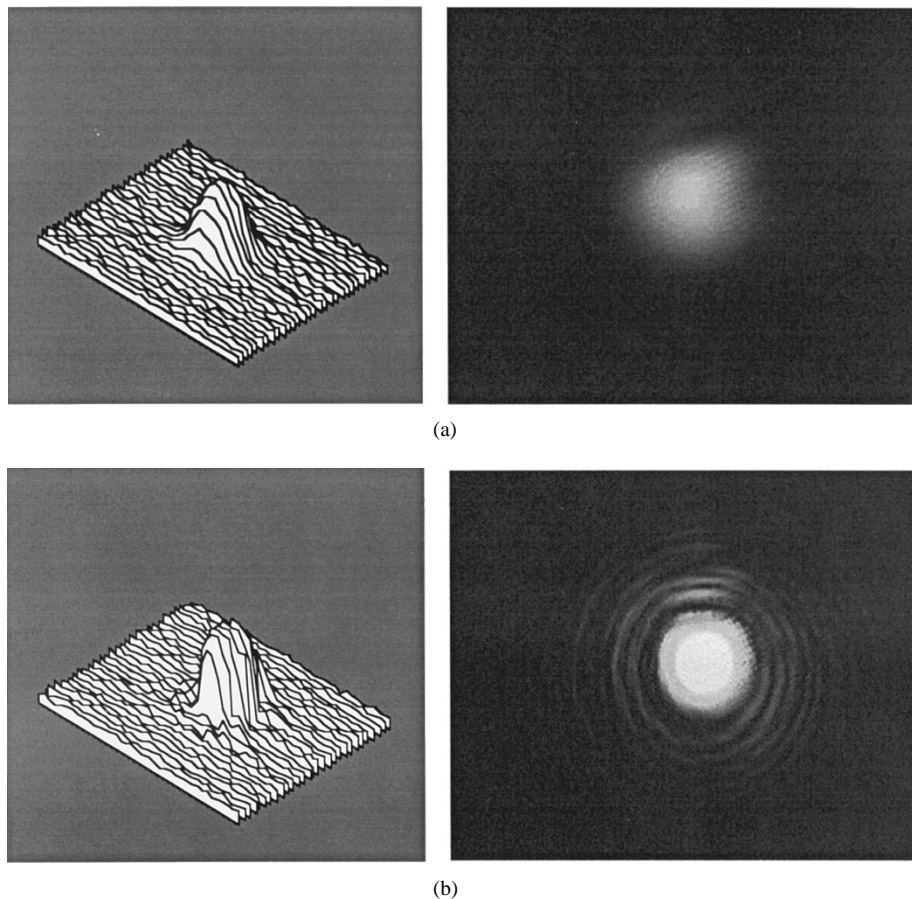


Fig. 13. Beam intensity profiles (left) and spot quality (right) from similar gratings fabricated on (a) unpolished and (b) polished polysilicon rotors.

and demonstrated. The effects of small (0.5-mm diameter) motor size and extraneous motor features (i.e., 50- μm diameter bearing) were found to be negligible upon the overall optical performance of the microscanner.

Dynamic Optical Performance

Scanning operation was demonstrated using a laser beam incident on the microscanner. Multiple diffraction orders were visible at meter distances. The scanned beams were examined with a silicon photodiode and a digital oscilloscope. The uniformity of the scanned beams was measured over many revolutions of the microscanner. Fig. 14 shows a typical intensity profile for a salient-pole microscanner during stepping operation. As a reference, a signal synchronous to the excitation voltage of the scanner micromotor is superimposed. In stepping mode operation, the next phase in the micromotor excitation signal is triggered after the rotor aligns with the stator pole. The scanner micromotor was also run using the continuous mode micromotor controller reported in [11]. This controller uses a pulse overlap scheme with a pulswidth that is the same duration as the step transient rise time, such that the next phase in the excitation sequence is triggered before the rotor aligns and the initially excited phase is grounded. This results in the rotor being drawn to the next stator phase in the excitation sequence without reducing the speed or reversing directions.

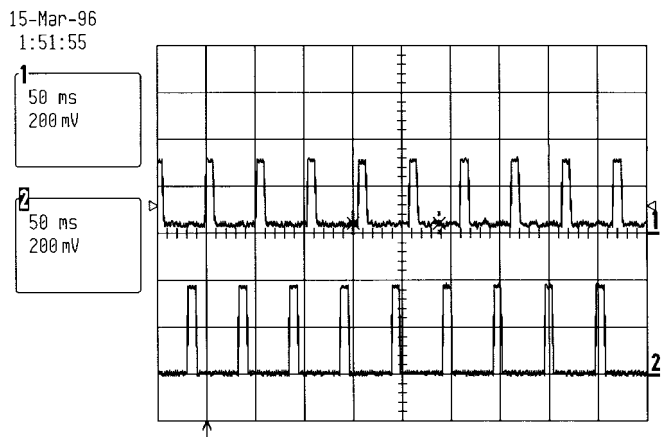


Fig. 14. Typical scan intensity measured during the operation of the microscanner (#1). As a reference, a signal synchronous to excitation signal of the scanner micromotor is superimposed (#2).

V. DISCUSSION

In the absence of a lens system, the trajectory of a given scanned spot during device operation is not straight and results in scan-line bow. For some applications, such as bar code reading, a finite amount of scan-line bow is not of a concern. However, for most other applications (e.g., imaging and printing) there are rigorous requirements on residual scan-line bow as a fraction of the scan-line length. In addition to

TABLE II
PERFORMANCE OF THE CURRENT DEVICE IN COMPARISON TO OTHER MICROMACHINED SCANNERS

Scanner Reported by	Scanning Approach	Actuation Method	Optical Efficiency	Scan Rate (scans/sec)	Angular Range	Power consumed
Current device	Diffraction grating motor	Electrostatic	5-7%*	347	360°	very low
Yasseen [3]	DRIE polygon motor	Electrostatic	12-27%	8	50-110°	very low
Kiang [12]	Flip-up resonating mirror	Electrostatic	?	3000	12°	very low
Schroth [13]	2D-deformable mirror	Piezoelectric	25%	35000	11-35°	low
Buhler [14]	1D-deformable mirror	Electrostatic	83-89%	?	9°	very low
Motamedi [15]	Bimorph cantilever	Thermal	90%?	2000	10-25°	high

* Absolute diffraction efficiency in the first order

a flat scanning plane, a decreased scanned spot diameter is desirable. This requires a pre-objective scanning lens system, where in addition to a laser focusing lens element placed after the input beam, lenses are placed between the scanner and the scanning plane. Special flat-field lenses must be used in order to focus the spot while permitting the beam motion along the lens diameter. Flat-field lenses typically consist of a negative lens followed by one or more positive lenses.

Device performance in comparison to the major microscanning approaches reported in literature is shown in Table II. The optical efficiency of the scanner is limited by the diffraction efficiency of the grating element and the reflectivity of polysilicon. With proper reflective coatings (e.g., 1000 Å of aluminum), the reflectance of these can be increased from 30% for Si up to 90% with Al coating. Commercial holographic scanners that employ grating elements can routinely achieve above 90% absolute diffraction efficiency in the first order. It is possible to get high diffraction efficiency on this device using a surface relief medium but, given a typical 633-nm light wavelength used in optical scanning, this may require submicron grating periods with relatively high aspect ratio relief profiles.

The scanner achieved scan speeds up to 347 scans per second which is suitable for many applications. The scan speed can be potentially increased by using more optimum drive electronics and by proper device packaging (e.g., in vacuum). Such packaging can reduce the effect of viscous drag components and allow for higher rotational speeds.

VI. CONCLUSION

Laser beam scanning using diffraction element microscanners was demonstrated. The diffraction elements were fabricated on the polished rotors of polysilicon surface micromachined, large-area micromotors. The reduced surface roughness provided by CMP enhanced feature definition and delineation in polysilicon and significantly improved the optical performance of the diffraction elements fabricated on polysilicon. High-quality diffraction beam profiles indicated that polished polysilicon is a viable material for production of low-cost high-quality microscanners. The fabricated diffraction elements were tested at visible wavelengths and were

verified to have spatial periods closely matching their design. Self-assembled monolayers were found to improve the scanner micromotors' reliability and overall dynamic performance characteristics. Stepping and continuous mode operation of the microscanner was demonstrated with visible diffraction orders at meter distances away. Continuous-mode operation was found to be more suitable for high-speed scanning applications.

ACKNOWLEDGMENT

The authors would like to thank G. Ramanathan and Dr. T. Pan for their contributions to this work.

REFERENCES

- [1] G. F. Marshall, *Optical Scanning*. New York: Marcel Dekker, Inc., 1991.
- [2] K. Deng, H. Miyajima, V. Dhuler, M. Mehregany, S. W. Smith, F. L. Merat, and S. Furukawa, "The development of polysilicon micromotors for optical microscanner applications," in *Tech. Dig., IEEE Solid-State Sensors and Actuators Workshop*, Hilton Head, SC, June 1994, pp. 234-238.
- [3] A. A. Yasseen, J. N. Mitchell, D. A. Smith, and M. Mehregany, "High-aspect-ratio rotary polygon micromotor scanners," in *Tech. Dig., IEEE Solid State Sensors and Actuators Workshop*, Hilton Head, SC, June 1998, pp. 75-78.
- [4] M. Mehregany and Y. C. Tai, "Surface micromachined mechanisms and micromotors," *J. of Micromechanics and Microengineering*, vol. 1, pp. 73-85, June 1992.
- [5] A. A. Yasseen, S. W. Smith, M. Mehregany, and F. L. Merat, "Diffraction grating scanners using polysilicon micromotors," in *Proc. IEEE Micro Electro Mechanical Systems*, Amsterdam, The Netherlands, Feb. 1995, pp. 175-180.
- [6] O. Slogaard, F. S. A. Sandejas, and D. M. Bloom, "Deformable grating optical modulator," *Opt. Lett.*, vol. 17, pp. 688-690, May 1992.
- [7] M. C. Hutley, *Diffraction Gratings*. London, U.K.: Academic, 1982.
- [8] K. Deng, M. Mehregany, and A. S. Dewa, "A simple fabrication process for side-drive micromotors," in *Tech. Dig., 7th Int. Conf. Solid-State Sensors and Actuators*, Yokohama, Japan, June 1993, pp. 756-759.
- [9] A. A. Yasseen, N. J. Mourlas, and M. Mehregany, "Chemical mechanical polishing for polysilicon surface micromachining," *J. Electrochem. Soc.*, vol. 144, no. 1, pp. 237-242, Jan. 1997.
- [10] K. Deng, R. Collins, M. Mehregany, and C. Sukenik, "Performance impact of monolayer coating of polysilicon micromotors," in *Proc. IEEE Micro Electro Mechanical Systems*, Amsterdam, The Netherlands, Feb. 1995, pp. 368-373.
- [11] N. J. Mourlas, K. C. Stark, M. Mehregany, and S. M. Phillips, "Exploring polysilicon micromotors for data storage micro disks," in *Proceedings, IEEE Micro Electro Mechanical Systems*, San Diego, CA, Feb. 1996, pp. 198-203.
- [12] M. H. Kiang, O. Solgaard, R. S. Muller, and K. Y. Lau, "Surface-micromachined electrostatic-comb driven scanning micromirrors for

barcode scanners," in *Proc. IEEE Micro Electro Mechanical Systems*, San Diego, CA, Feb. 1996, pp. 192–197.

- [13] A. Scroth, C. Lee, S. Matsumoto, M. Tanaka, and R. Maeda, "Application of Sol-Gel deposited thin PZT film for actuation of 1D and 2D scanners," in *Proc. IEEE Micro Electro Mechanical Systems*, Heidelberg, Germany, Feb. 1998, pp. 402–707.
- [14] J. Bhuler, F. Steiner, R. Hauert, and H. Baltes, "Linear array of complementary metal oxide semiconductor double-pass metal micromirrors," *Opt. Eng.*, vol. 36, no. 5, pp. 1391–1398, May 1997.
- [15] M. E. Motamedi, S. Park, A. Wang, M. S. Dadkhah, A. P. Andrews, H. O. Marcy, M. Khoshnevisan, A. E. Chiou, R. J. Huhn, C. F. Sell, and J. G. Smits, "Development of micro-electro-mechanical optical scanner," *Opt. Eng.*, vol. 36, no. 5, pp. 1346–1351, May 1997.

A. Azzam Yasseen, for photograph and biography, see this issue, p. 31.



Steven W. Smith received the B.S. degree in applied physics and the M.S. degree in electrical engineering, both from Case Western Reserve University.

From 1996 to 1998, he worked as a Display Engineer at Kent State University's Liquid Crystal Institute and is currently employed at Motorola's Personal Communications Sector. He is a product development engineer responsible for electrical and optical design of information displays for personal communications devices.



Francis L. Merat (S'73–M'77) was born in Frenchville, PA, in August 1949. He received the B.S. degree in electrical engineering and applied physics from Case Institute of Technology in 1972 and the M.S. and Ph.D. degrees in electrical engineering and applied physics from Case Western Reserve University, Cleveland, OH, in 1975 and 1978, respectively.

In 1979, he joined Case Western Reserve University as an Assistant Professor. He is now an Associate Professor of Electrical Engineering.

His current research interests include neural network applications to image and signal processing, agile manufacturing, industrial inspection and sensing, optical MEMS, and wireless communications. His teaching interests include digital and analog electronics, and embedded microprocessor systems as well as courses in optics, wireless communications, and image processing. He is the author or co-author of 14 journal publications, 51 conference publications, and two book chapters.

Dr. Merat is a member of Sigma Xi, ACM, SME, and ASEE. He received the National Association for Academic Counseling and Advising Distinguished Advisor Award in 1985 and the 1996 Y. H. Pao Best Paper Award for Innovative Neural Network Applications in 1996.

Mehran Mehregany (S'88–M'92), for photograph and biography, see this issue, p. 32.